


Inference of parameters for the back-shifted Fermi gas model using a feedforward neural networkPeng-Xiang Du , Tian-Shuai Shang , Kun-Peng Geng, and Jian Li ^{*}
*College of Physics, Jilin University, Changchun 130012, China*Dong-Liang Fang 
Institute of Modern Physics, Chinese Academy of Sciences, Lanzhou 730000, China

(Received 12 January 2024; accepted 25 March 2024; published 24 April 2024)

The back-shifted Fermi gas model is widely employed for calculating nuclear level density (NLD) as it can effectively reproduce experimental data by adjusting parameters. However, selecting parameters for nuclei lacking experimental data poses a challenge. In this study, a feedforward neural network (FNN) was utilized to learn the level density parameters at neutron separation energy $a(S_n)$ and the energy shift Δ for 289 nuclei. Simultaneously, parameters for nearly 3000 nuclei are provided through the FNN. Using these parameters, calculations were performed for neutron resonance spacing in s and p waves, cumulative number of levels, and NLD. The FNN results were also compared with the calculated outcomes of the parameters from fitting experimental data (local parameters) and those obtained from systematic studies (global parameters), as well as the experimental data. The results indicate that parameters from the FNN achieve performance comparable to local parameters in reproducing experimental data. Moreover, for extrapolated nuclei, parameters from the FNN still offer a robust description of experimental data.

DOI: [10.1103/PhysRevC.109.044325](https://doi.org/10.1103/PhysRevC.109.044325)**I. INTRODUCTION**

Nuclear level density (NLD) constitutes a fundamental input parameter in the calculation of nuclear reaction cross sections using statistical models, such as the Hauser-Feshbach formula [1,2]. Specifically, in instances where discrete-level information is incomplete or unavailable at a given excitation energy, the level density is employed to calculate the corresponding transmission coefficients. In nuclear reactions involving compound nuclear processes, including capture reactions and fission reactions, knowledge of the level density is of crucial importance [3,4]. It significantly impacts the calculations of nucleosynthesis in various astrophysical environments and also has substantial implications for the assessment of nuclear fission yields.

NLD is a physical quantity whose direct measurement is challenging. Meanwhile, the most abundant data are from indirect measurements including the cumulative number of discrete levels at low excitation energy and neutron resonance spacing. As an alternative, the Oslo method, progressively developed in recent years, can extract the γ strength function and level density from the γ spectra of specific reactions [5–8]. However, the NLD data from this technique remain limited.

The earliest theoretical calculations of NLD conducted by Hans Bethe provided a simple analytical expression for the level density using the noninteracting Fermi gas model [9,10]. Based on such calculations and considering shell effects and

pairing effects, a series of phenomenological models have been developed, including the constant temperature model (CTM) [11], the back-shifted Fermi gas model (BFM) [12], and the generalized superfluid model (GSM) [13]. Meanwhile, in the past few decades, various microscopic methods based on mean-field approximation or shell models have also been developed to describe NLD. Methods based on mean-field approximations include combinatorial methods [14–20] and microscopic statistical methods [21–26]. Calculations based on the shell model have also been attempted [27,28]. To avoid the substantial computational complexity associated with diagonalizing a massive Hamiltonian, many methods such as the Monte Carlo shell model method [29–32], stochastic estimation method [33,34], moments method [35,36], and the Lanczos method [37] have been developed. Shell model methods are constrained by the complexity of diagonalizing the Hamiltonian, making it challenging to conduct large-scale calculations for the entire nuclide chart. Combinatorial methods have now achieved a precision level close to that of phenomenological models. Recently, a new approach based on the boson expansion of QRPA excitations was proposed [38]. Despite the availability of numerous microscopic methods for calculating NLD, phenomenological models, owing to their simplicity and rapid computational capabilities, continue to be widely employed in various nuclear reaction calculations. For nuclei with discrete levels and s -wave neutron resonance spacings (D_0), phenomenological models can effectively reproduce experimental data by adjusting parameters. According to recent results of fitting parameter, the BFM exhibits slightly better performance in reproducing experimental data on D_0 compared to CTM and GSM [39].

^{*}jianli@jlu.edu.cn

The BFM primarily utilizes two adjustable parameters, i.e., level density parameter a and energy shift Δ to obtain NLD. In earlier fitted results, Δ was found to be negative for all odd-odd nuclei, corresponding to a downward shift of the ground-state energy by 1–3 MeV; it is referred to as the back-shifted Fermi gas model [12,40]. In the subsequent developments, to account for the damping of shell effects with increasing excitation energy, the level density parameter a was modified to be a function of excitation energy [13]. To address the divergence issue of the original BFM at low energies, an extra term denoted as ρ_0 —which is related to the level density parameter a , energy shift Δ , and spin cutoff parameter σ^2 —has been added to the expression for the total nuclear level density [24,41]. Based on these adjustments, the level density parameters (local parameters), $a(S_n)$ (a at the neutron separation energy S_n) and Δ , for 289 nuclei were determined by fitting experimental data on D_0 and discrete levels [39]. Subsequently, a set of global parameters are derived through systematic investigation to describe NLD of nuclei lacking experimental data [39]. The determined local parameters through fitted experimental data exhibit complex variations, and also implicitly reflect shell effects, pairing effects, and other effects. Therefore, it is crucial to adopt reliable methods for describing the trends of these parameters and offering reasonable extrapolations for isotopes with limited experimental data [39,42,43].

In recent years, machine learning has been increasingly applied across the area of nuclear physics, covering various topics such as nuclear data, nuclear theory, experimental methods, and accelerator technology [44–46]. Specifically, machine learning techniques have been widely used as research tools in areas including nuclear mass [47–52], nuclear charge distribution [53–56], β -decay half-lives [57,58], giant dipole resonance [59,60], magnetic moment [61], ground-state spin [62], low-lying excitation spectra [63,64], reaction cross-sections [65,66], wave functions of light nuclei [67,68], neutron star equation of state [69], etc. These results demonstrate its capabilities in data processing and predictions of various measurements. In the study of nuclear level density, a Bayesian neural network has been employed to train the level density parameter a from RIPL-2 for CTM, BFM, and GSM [70]. Energy shifts were not involved in this work, and no extrapolation of the data was conducted. However, this is a valuable attempt that demonstrates the feasibility of utilizing machine learning to investigate the variation patterns of level density parameters. On the other hand, Ref. [43] conducted a systematic study and proposed a simple expression related to shell effects to calculate energy shifts. It suggests that the changes in the parameter Δ follow a pattern that can be captured by machine learning. Among various machine learning models, the feedforward neural network (FNN) is widely utilized by nuclear physicists due to its simple structure, strong interpretability, and powerful data fitting capabilities [55,56,71–74]. Therefore, we employ the FNN to learn and extrapolate the level density parameter and energy shift of the BFM, to enable the prediction of nuclear level density.

The article is arranged as follows. The details of BFM and FNN are discussed in Sec. II. Section III evaluates the parameters a and Δ obtained from the FNN, and employs these

parameters for extensive verification calculations, including neutron resonance spacings, cumulative number of levels, and level densities. Section IV provides a summary and offers some perspectives.

II. THE BACK-SHIFTED FERMI GAS MODEL AND THE FEEDFORWARD NEURAL NETWORK

A. The back-shifted Fermi gas model

According to BFM [12,39], the total nuclear level density for a given excitation energy E_x can be expressed as

$$\rho_{\text{BFM}}^{\text{tot}}(E_x) = \left[\frac{1}{\rho(E_x)} + \frac{1}{\rho_0(E_x)} \right]^{-1}, \quad (1)$$

where $\rho(E_x)$ is given by

$$\rho(E_x) = \frac{1}{\sqrt{2\pi}\sigma} \frac{\sqrt{\pi}}{12} \frac{\exp[2\sqrt{aU}]}{a^{\frac{1}{4}} U^{\frac{5}{4}}}, \quad (2)$$

and the expression for the second term is

$$\rho_0(E_x) = \frac{\exp(1)a}{12\sigma} \exp(aU). \quad (3)$$

In this context, both the level density parameter a and the spin cutoff parameter σ^2 are functions of energy, and the effective excitation energy U is given by $U = E_x - \Delta$.

For the level density parameter a , it can be expressed in the following form [13]:

$$a(E_x) = \tilde{a} \left(1 + \delta W \frac{1 - \exp[-\gamma U]}{U} \right). \quad (4)$$

Here, \tilde{a} is the asymptotic level density value that one would obtain in the absence of any shell effects, and it can be parametrized as a function of the mass number A , written as

$$\tilde{a} = \alpha A + \beta A^{\frac{2}{3}}. \quad (5)$$

δW is the shell correction term, defined as the difference between the experimental nuclear mass and the liquid-drop model mass. γ is a parameter used to describe the decay of shell effects with increasing energy, expressed as

$$\gamma = \frac{\gamma_1}{A^{\frac{1}{3}}}. \quad (6)$$

For the energy shift Δ , the expression is as follows:

$$\Delta = \begin{cases} \frac{12}{\sqrt{A}} + \delta & \text{for even-even,} \\ -\frac{12}{\sqrt{A}} + \delta & \text{for odd-odd,} \\ \delta & \text{for odd-A.} \end{cases} \quad (7)$$

In the calculations of this study, for convenience, the spin-cutoff parameter σ^2 is expressed in the form of the following piecewise function:

$$\sigma^2 = \begin{cases} \sigma_d^2 & \text{for } E_x \leq \Delta, \\ \sigma_d^2 + \frac{E_x - \Delta}{S_n - \Delta} [\sigma_F^2(E_x) - \sigma_d^2] & \text{for } \Delta < E_x < S_n, \\ \sigma_F^2(E_x) & \text{for } E_x \geq S_n, \end{cases} \quad (8)$$

where σ_d^2 is represented as

$$\sigma_d^2 = (0.83A^{0.26})^2, \quad (9)$$

and $\sigma_F^2(E_x)$ is

$$\sigma_F^2(E_x) = 0.01389 \frac{A^{5/3}}{\bar{a}} \sqrt{aU}. \quad (10)$$

Finally, taking into account the parity and spin distributions, the level density is expressed as

$$\rho(U, J, P) = \frac{1}{2} \frac{2J+1}{2\sigma^2} \exp\left[-\frac{(J+\frac{1}{2})^2}{2\sigma^2}\right] \rho_{\text{BFM}}^{\text{tot}}(E_x). \quad (11)$$

On this basis, neutron resonance spacings and the cumulative number of levels can also be calculated.

B. The feedforward neural network

The FNN consist of multiple layers, including the input layer, hidden layers, and output layer. Each layer contains multiple neurons. Neurons receive incoming information and pass it to the next layer through an activation function. The information ultimately reaches the output layer, completing the data processing.

In this study, the hyperbolic tangent function (tanh) is chosen as the activation function for the FNN hidden layer, and the mean square error (MSE) is selected as the loss function for the network, expressed as

$$\text{Loss} = \frac{1}{N_t} \sum_{i=1}^{N_t} (y_{\text{tar}} - y_{\text{pre}})^2, \quad (12)$$

where N_t represents the size of the dataset, y_{tar} represents the fitted values, and y_{pre} represents the predictions given by the FNN. During the network training process, the stochastic gradient descent method [75] is applied to continuously update the network parameters in order to minimize the loss function.

The data utilized in this study comprise level density parameters at the neutron separation energy $a(S_n)$ and energy shifts Δ for 289 nuclei. These data are obtained by fitting the D_0 and discrete levels in RIPL-2 [39]. The corresponding dataset can be found in the data files of TALYS version 1.8 and above [76]. It is important to note that δ values are provided for an additional 846 nuclei with only discrete level data. However, to ensure the consistency of the utilized data, these values were not used to train the neural network.

In view of the intricate relationship between $a(S_n)$ and δ , and the overall lack of strong regularity in δ , the dataset underwent classification. Utilizing Eq. (7) to transform δ back to Δ , the training of the network was conducted separately for $a(S_n)$ and Δ . Additionally, the Δ dataset was categorized into three classes: even-even nuclei, odd-odd nuclei, and odd- A nuclei, and each was used for training the network. For $a(S_n)$, it explicitly includes the neutron separation energy S_n in Eq. (4), and when expressed as a function of the mass number A it exhibits pronounced shell effects. Therefore, the proton number Z , neutron number N , the difference between each of them and the nearest magic numbers (V_z , V_n), as well as the neutron separation energy S_n are chosen as input variables

TABLE I. The statistical analysis of the MSE for 100 sets of training outcomes across four neural networks includes assessments on both the training and validation sets. ‘‘SD’’ denotes the sample standard deviation.

Target	Mean (training set)	SD	Mean (validation set)	SD
$a(S_n)$	0.55	0.18	0.80	0.17
$\Delta^{\text{even-even}}$	0.04	0.02	0.05	0.02
$\Delta^{\text{odd-odd}}$	0.14	0.13	0.10	0.08
$\Delta^{\text{odd-A}}$	0.12	0.08	0.12	0.05

for the FNN. After grid search, the final decision is a double-hidden-layer network, with each layer containing 32 neurons. As for Δ , the selected input variables for the network are Z , N , V_z , and V_n . The FNN models for even-even nuclei and odd-odd nuclei both have two hidden layers with 35 neurons and 10 neurons per layer, while a single hidden layer with 26 neurons is employed for odd- A nuclei.

During training, the data are randomly divided into a training set and a validation set, with the training set accounting for 80% of the data and the validation set for 20%. FNN parameters are randomly initialized for each training iteration. In order to capture all features of the original data while minimizing the MSE, each network undergoes 1000 repetitions of training. The final results for $a(S_n)$ and Δ are obtained by averaging the 100 sets of data provided by the FNN, with the smallest MSE. The performances of each neural network on the training and validation sets are provided in Table I. These results indicate the rationality of employing the current hyperparameters for training neural networks.

III. RESULTS AND DISCUSSION

Figure 1 depicts the values of $a(S_n)$ provided by the FNN for all 289 nuclei. In addition, the results of parameters fitted

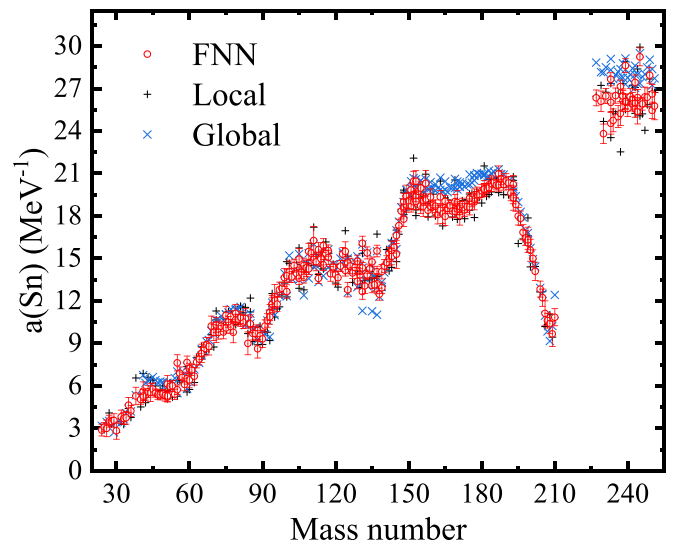


FIG. 1. Level density parameters a at the neutron separation energy S_n . The parameters obtained from the FNN (red circles with error bars) and global parameters (blue crosses) were compared with the local parameters (black crosses).

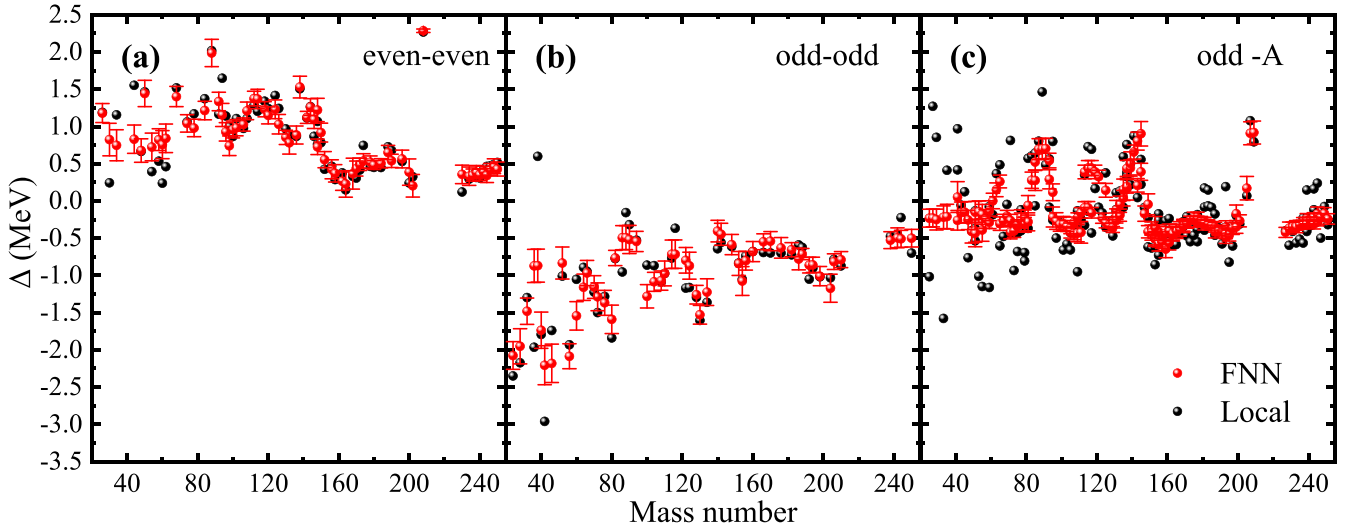


FIG. 2. The energy shift Δ for even-even nuclei, odd-odd nuclei, and odd-A nuclei. The parameters obtained from the FNN (red spheres with error bars) were compared with the local values (black spheres).

to experimental data (local parameters) and global parameters are also presented for comparison. The error bars in the FNN results are derived from twice the standard deviation of multiple training outcomes, indicating that approximately 95% of the data fall within the range of the error bars. It is evident that the FNN effectively captures the variation patterns in the local parameters $a(S_n)$, especially for nuclei with mass number above 150, where global parameters clearly provide overestimated predictions. Overall, the FNN yields a root-mean-square deviation of 0.67, significantly outperforming the global parameters with a deviation of 1.18.

Regarding Δ , the results of FNN training are presented in Fig. 2. Error bars are also provided at two times the standard deviation. In the dataset, there are 67 even-even nuclei, 56 odd-odd nuclei, and 166 odd-A nuclei. The FNN yields root-mean-square deviations of 0.20, 0.33, and 0.36 for the above categories, respectively. It can be observed that, whether it is an even-even, odd-odd or odd-A nucleus, the absolute value of Δ continuously oscillates and tends towards zero with an increase in the mass number. Meanwhile, variations in the values of Δ are evident around magic numbers. This underscores a clear fact that the Fermi gas model is better suited for describing systems with a larger number of nucleons. For light nuclei, however, larger parameter adjustments are necessary to align with experimental data. In general, for both even-even and odd-odd nuclei, the FNN effectively reproduces the changing trends of Δ . The inclusion of magic number information in the network inputs allows FNN to capture the associated variations. For instance, in Fig. 2(a), the case of ^{208}Pb clearly deviates from the overall trend, but FNN accurately describes its results. Another notable fact is that FNN's description of Δ for medium-heavy nuclei is significantly better than for light nuclei. The primary reason is the extremely pronounced variations of Δ in the light nuclei region, and these variations do not exhibit a clear connection to magic number information. Additionally, the amount of data used to train the network in the light nuclei region is relatively limited. For example, in Fig. 2(b), the case of ^{38}Cl exhibits local values

that are positive, making it challenging for FNN to capture such variations. Especially for odd-A nuclei, FNN can roughly describe the patterns of local values in the region above mass number 80, but struggles to capture these oscillations below mass number 80.

D_0 values are the most reliable experimental data related to NLD. Figure 3 depicts the ratio of calculated D_0 , using parameters obtained from FNN, to the corresponding experimental values from RIPL-2. Meanwhile, the results of calculations using local parameters and global parameters are also given separately. Due to the absence of D_0 for ^{251}Cf in RIPL-3, subsequent comparisons did not consider this nucleus. It can be observed that, for both even-even and odd-odd nuclei, the calculated results for all three sets of parameters mostly fall within a range of 0.5 to 2 times the experimental values. For odd-A nuclei, the calculated results using local parameters mostly cluster around two times the experimental values, while the results from FNN parameters and global parameters are scattered above and below the dashed line representing two times the experimental values.

The differences in the calculated results for the three types of parameters, i.e., local, global, and FNN are revealed through the root-mean-square deviation factor, denoted as f_{rms} , between the theoretical and experimental values of D_0 . f_{rms} is defined as follows [14]:

$$f_{\text{rms}} = \exp \left[\frac{1}{N_e} \sum_{i=1}^{N_e} \ln^2 \frac{D_0^{\text{th}}}{D_0^{\text{exp}}} \right]^{1/2}, \quad (13)$$

where N_e is the number of nuclei considered. The corresponding results are provided in Table II. In an overall assessment, the parameters obtained from FNN yield a value of $f_{\text{rms}} = 1.87$, which is bigger than the local parameters (1.76) but superior to the global parameters (2.22). This result is consistent with its performance in both even-even and odd-odd nuclei. However, for odd-A nuclei, the parameters from FNN yield a value of $f_{\text{rms}} = 2.04$, even slightly surpassing the local parameters (2.05) and significantly outperforming the global

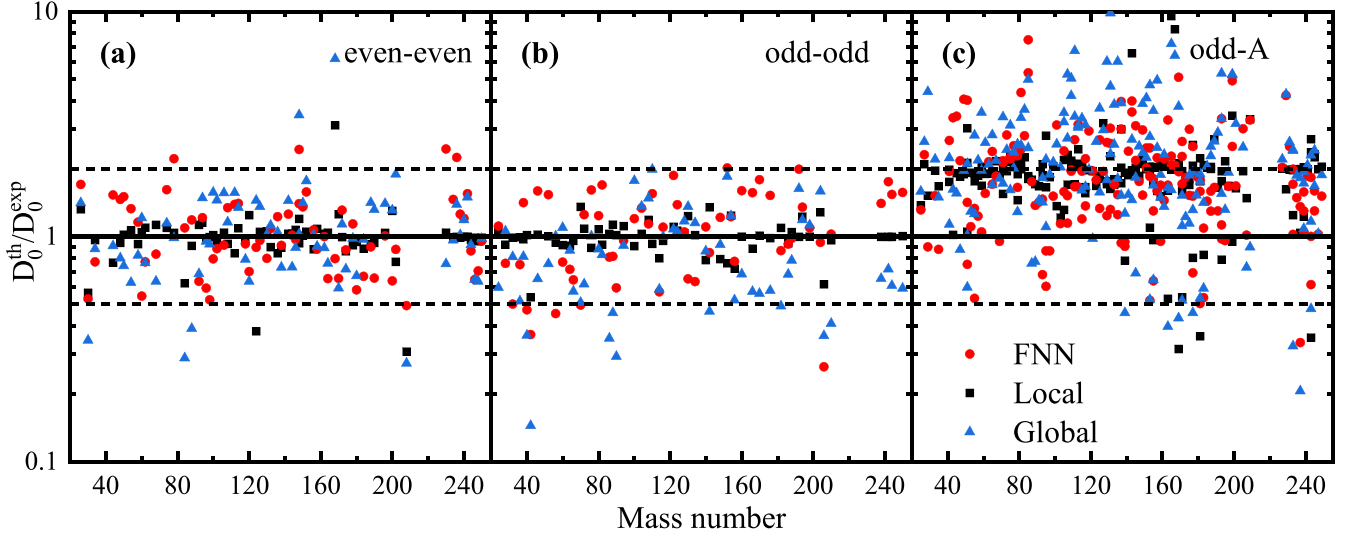


FIG. 3. The ratio of the s -wave neutron resonance spacings D_0 predicted by the BFM for even-even, odd-odd, and odd- A nuclei to the experimental data from RIPL-2 as a function of mass number A . The parameters obtained from the FNN (red circles) and global parameters (blue triangles) were compared with the local parameters (black squares).

parameters (2.59). From Fig. 3(c), it can be observed that the results from FNN are more scattered, with a larger proportion falling below the dashed line representing twice the experimental values.

Given the outstanding performance of FNN on the original dataset of 289 nuclei mentioned above, the same approach is employed to extensively extrapolate $a(S_n)$ and Δ , providing parameters for 2882 nuclei beyond the dataset. Specific parameters are provided in the Supplemental Material [77], with the extrapolation range covering Z from 1 to 118 and N from 1 to 177. In the input of FNN, $Z = 126$ and $N = 184$ are set to magic numbers. The ground-state information for all these nuclei can be found in RIPL-3, and this information is assumed to be entirely correct. Subsequently, these ground-state level properties, along with the parameters obtained from FNN, are used to calculate D_0 . The corresponding results are presented in Fig. 4(a). The calculated results show that (1) within an isotopic chain, D_0 generally increases with an increase in neutron numbers, (2) the nuclei near magic numbers exhibit larger D_0 values compared to their surrounding nuclei, (3) there is a clear odd-even effect in the calculated results, where even-even nuclei within the isotopic chain typically possess smaller D_0 values compared to nearby odd- A nuclei.

TABLE II. The root-mean-square deviation factor f_{rms} for D_0 values obtained through BFM calculations using FNN parameters, local parameters, and global parameters, in comparison to the experimental data in RIPL-2.

Parameter types	$f_{\text{rms}}^{\text{even-even}}$ 67 nuclei	$f_{\text{rms}}^{\text{odd-odd}}$ 56 nuclei	$f_{\text{rms}}^{\text{odd-A}}$ 165 nuclei	$f_{\text{rms}}^{\text{Entirety}}$ 288 nuclei
FNN	1.46	1.58	2.04	1.87
Local	1.31	1.18	2.05	1.76
Global	1.62	1.76	2.59	2.22

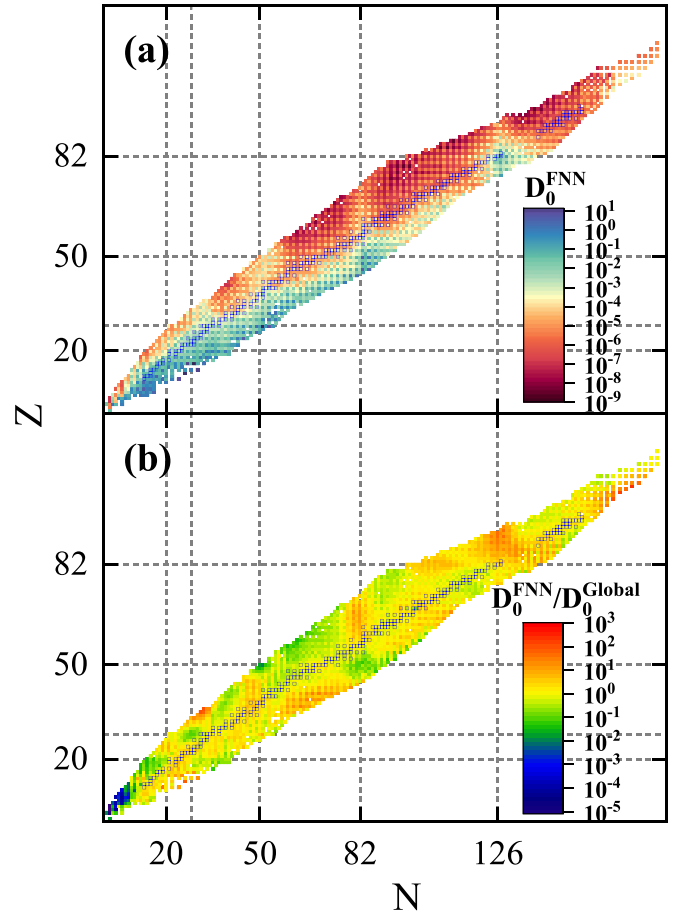


FIG. 4. The D_0 values calculated using parameters from FNN (a) and their ratios to the results obtained from global parameters (b) for 3171 nuclei, including 289 nuclei within the dataset (represented by blue boxes) and 2882 nuclei outside the dataset.

It is also necessary to compare the present level parameters of FNN with the available global parameters, their ratios, i.e., $D_0^{\text{FNN}}/D_0^{\text{Global}}$, are shown in Fig. 4(b). Figure 4(b) shows the ratios of D_0 calculated from FNN parameters to the results obtained from global parameters. It can be observed that the discrepancies between the FNN and global parameters results are within an order of magnitude within most regions of the nuclide chart. It is noteworthy that, in the vicinity of ^{100}Sn and ^{132}Sn , the FNN consistently yields smaller predictive results. By comparing the values of $a(S_n)$ obtained through the two methods, around ^{100}Sn and ^{132}Sn , the $a(S_n)$ values calculated using global parameters tend to be smaller than the predictions from FNN. This difference will lead to larger values of D_0 . The reason for this phenomenon could be the stronger shell correction (δW) in this region. For nuclei distributed along the dashed lines representing the magic numbers $Z = 82$, $N = 82$, and 126 (excluding those near ^{132}Sn), the FNN provides predictive results that are larger than those obtained with global parameters. One possible reason for such discrepancies could be that FNN, due to the input of magic number information, predicts stronger shell effects in these regions. Additionally, for light proton-rich nuclei (especially ^{14}O and its vicinity), the predictions of the FNN and the global parameters reveal significant differences. These variations beyond the dataset are entirely beyond the grasp of FNN. The true nature is yet to be revealed through subsequent experimental observations.

RIPL-3 has incorporated D_0 data for more nuclei compared to RIPL-2, and also provided updates to the D_0 values for some previously included nuclei [40]. The presence of D_0 values for 12 nuclei in RIPL-3, not included in the original dataset, provides an opportunity to evaluate the validity of the parameters from FNN. The target nuclei corresponding to these D_0 values include ^{30}Si , ^{86}Kr , ^{96}Zr , ^{100}Ru , ^{122}Sn , ^{134}Cs , ^{135}Cs , ^{133}Ba , ^{153}Gd , ^{231}Pa , ^{233}Pa , and ^{252}Cf . The ratios of D_0 values calculated using FNN to experimental data are presented in Fig. 5. The results obtained using global parameters are also given simultaneously. Overall, the results from FNN are distributed in the range of 0.5 to 2, with the minimum value being 0.31 (^{154}Gd) and the maximum value being 2.45 (^{232}Pa). In comparison to global parameters, FNN's results are superior for nuclei with mass numbers below 200, while FNN's results are slightly inferior for the three nuclei with mass numbers above 200. In general, the parameters obtained from FNN yield a value of $f_{\text{rms}} = 1.98$, and the global parameters similarly give 1.98 in this context. Despite the D_0 updates in RIPL-3 compared to RIPL-2, the parameters from FNN consistently yield $f_{\text{rms}} = 1.98$ for the remaining 288 nuclei provided in RIPL-3. The obtained result is consistent with the outcomes for the predicted 12 nuclei. This, to some extent, indicates that the approach of extrapolating parameters using FNN is stable, at least for nuclei close to the original dataset. In contrast, the global parameters yield $f_{\text{rms}} = 2.19$ for the remaining 288 nuclei in RIPL-3.

Moreover, the p -wave neutron resonance spacing D_1 also can be used to evaluate the quality of parameters. RIPL-3 provides D_1 values for 116 nuclei, including 18 even-even nuclei, 26 odd-odd nuclei, and 72 odd- A nuclei. The ratio of the calculated D_1 using parameters obtained from FNN to the

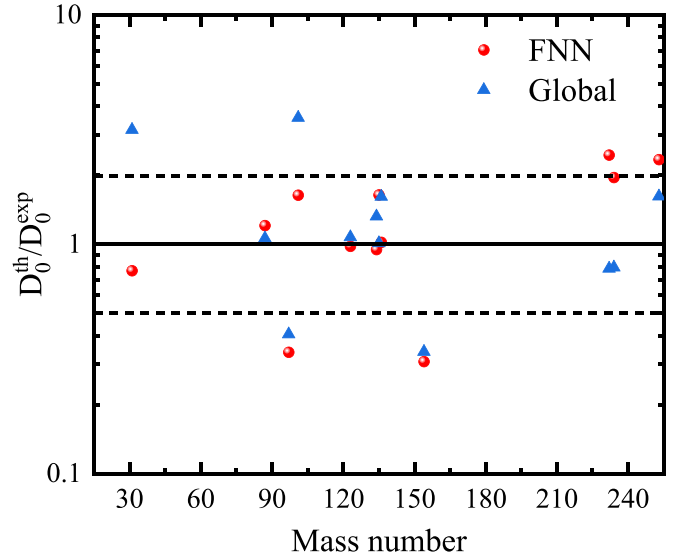


FIG. 5. The ratio of the D_0 values predicted by BFM for 12 nuclei outside the dataset to the experimental data in RIPL-3. The results obtained from FNN parameters (red spheres) were compared with the results from global parameters (blue triangles).

experimental data from RIPL-3 is presented in Fig. 6. The results from local parameters and global parameters are also displayed for comparison. It can be observed that, unlike the case of D_0 , the results of calculations using local parameters are no longer widely distributed along lines representing 1 or 2. Instead, similarly to FNN parameters and global parameters, they are scattered between 0.5 and 2 times the experimental values. Similarly to Eq. (13), the corresponding root mean square deviation is provided in Table III. For even-even and odd-odd nuclei, the calculated results from FNN parameters yield f_{rms} bigger than local parameters but smaller than global parameters. However, for odd- A nuclei, the performance of FNN parameters is better than that of local parameters. In the end, for all 116 nuclei, FNN parameters yield $f_{\text{rms}} = 1.76$, which is slightly better than the 1.79 from local parameters and superior to the 1.92 from global parameters.

Discrete levels at low excitation energies are the most abundant experimental data related to NLD. In the process of fitting BFM parameters, it is observed that the cumulative number of levels is highly sensitive to variations in energy shift. Certainly, the cumulative count of discrete levels can be employed to validate the reasonableness of Δ obtained from FNN. Three isotopic chains, including Cu, Dy, and Pu,

TABLE III. The root-mean-square deviation factor f_{rms} for D_1 values calculated using different types of parameters compared to the experimental data in RIPL-3.

Parameter types	$f_{\text{rms}}^{\text{even-even}}$ 18 nuclei	$f_{\text{rms}}^{\text{odd-odd}}$ 26 nuclei	$f_{\text{rms}}^{\text{odd-}A}$ 72 nuclei	$f_{\text{rms}}^{\text{Entirety}}$ 116 nuclei
FNN	1.42	1.58	1.90	1.76
Local	1.40	1.41	2.01	1.79
Global	1.45	1.61	2.13	1.92

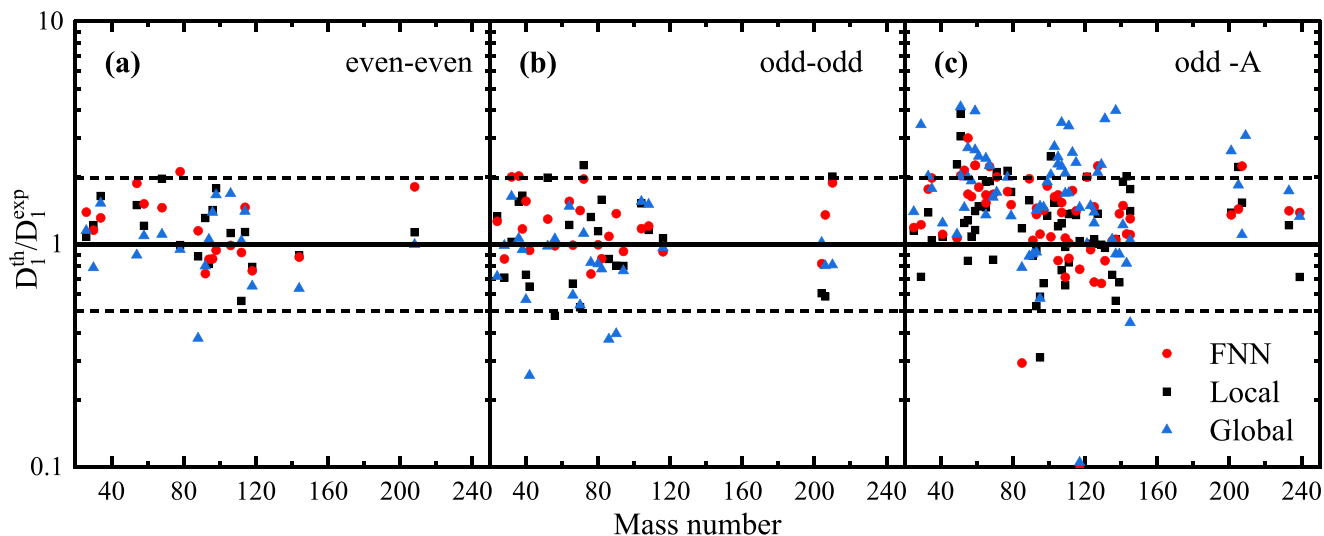


FIG. 6. The ratio of the p -wave neutron resonance spacings D_1 predicted by the BFM for even-even, odd-odd, and odd- A nuclei to the experimental data from RIPL-3 as a function of mass number A . The FNN parameters (red circles) and global parameters (blue triangles) were compared with the local parameters (black squares).

have been selected to validate the parameters obtained using FNN. Figure 7 displays the results of the cumulative number of levels from FNN for nuclei ranging from ^{58}Cu to ^{66}Cu . The corresponding results of global parameters are also provided. Additionally, for nuclei within the original dataset, results obtained using local parameters are presented. For the Cu isotopic chain, only ^{64}Cu and ^{66}Cu are within the dataset. From Fig. 7, it can be observed that the parameters provided by FNN fit well with the experimental data for ^{64}Cu and ^{66}Cu . For ^{64}Cu , the results even surpass the local parameters. Besides, for nuclei outside the dataset, FNN yields results superior to global parameters, particularly for $^{58-60}\text{Cu}$, which are more

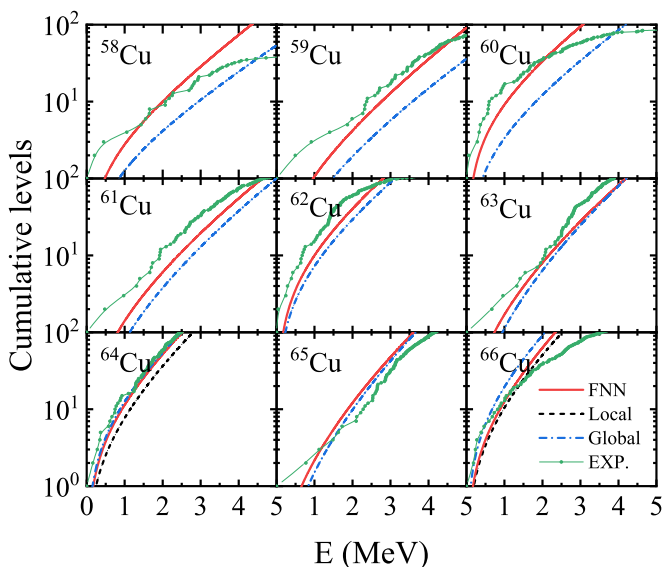


FIG. 7. Cumulative number of levels for $^{58-66}\text{Cu}$. Comparison was made between the results calculated from FNN parameters (red line), global parameters (blue dotted-dashed line), and local parameters (black dashed line), and the experimental data (green dot line).

distant from the dataset, demonstrating a good description by FNN.

Similarly to Fig. 7, Fig. 8 displays the calculated results of the cumulative number of levels for ^{155}Dy to ^{166}Dy . For nuclei within the dataset (^{157}Dy , ^{159}Dy , $^{161-165}\text{Dy}$), the results from FNN parameters are very close to those obtained with local parameters. Regarding the extrapolation results, FNN demonstrates strong predictive capabilities, effectively

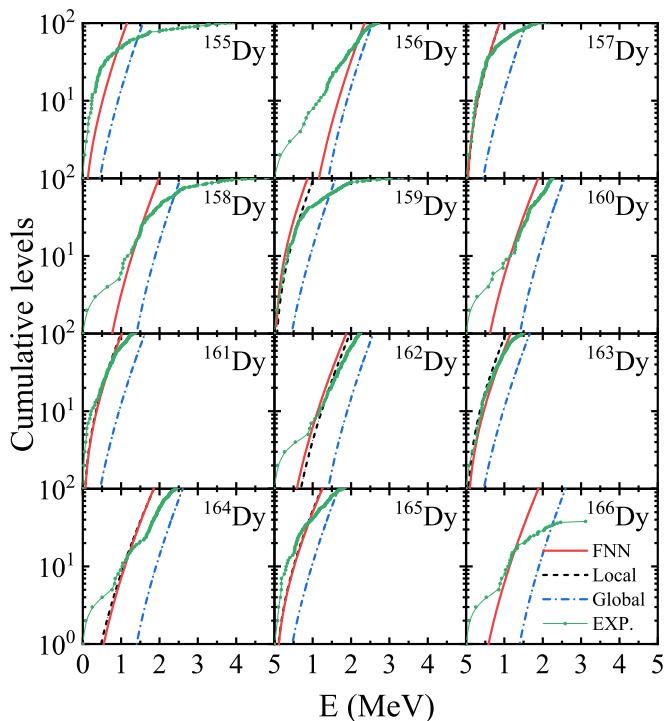


FIG. 8. The cumulative number of levels calculated with FNN parameters, local parameters, and global parameters are compared with the experimental data, for $^{155-166}\text{Dy}$.

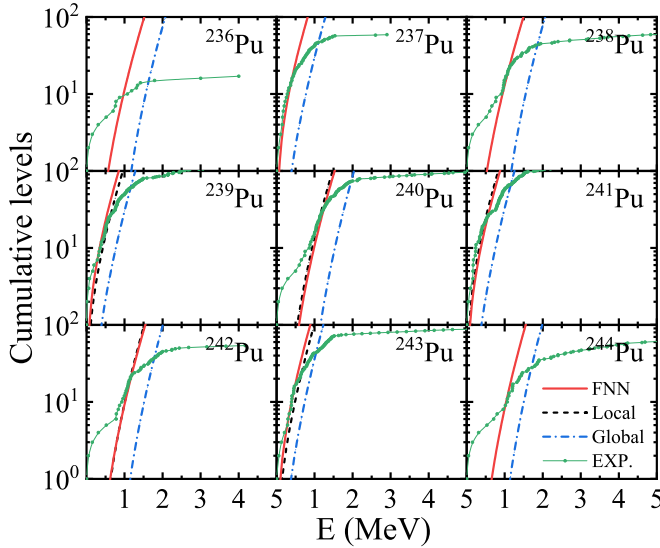


FIG. 9. The cumulative numbers of levels calculated with FNN parameters, local parameters, and global parameters are compared with the experimental data, for $^{236-244}\text{Pu}$.

reproducing the experimental results for ^{158}Dy , ^{160}Dy , and ^{166}Dy . Moreover, for ^{155}Dy and ^{156}Dy , FNN provides results superior to global parameters. The results for Pu isotopes from ^{236}Pu to ^{244}Pu are presented in Fig. 9. It can be observed that, for nuclei within the dataset ($^{239-243}\text{Pu}$), the parameters from FNN provide results that closely overlap with those from local parameters while effectively reproducing experimental data. Additionally, for extrapolated nuclei ($^{236-238}\text{Pu}$, ^{244}Pu), FNN parameters yield excellent agreement with experimental data. Overall, the parameters from FNN provide a good description of the cumulative number of levels for nuclei in these three chains, especially for nuclei outside the dataset where FNN still provides accurate predictions. This serves as strong evidence for the reliability of the Δ obtained from FNN.

Finally, the comparison between the calculated results of the NLD using FNN parameters for the 12 nuclei between ^{51}V to ^{207}Pb and Oslo data [78–87] is presented in Fig. 10. The results obtained using global parameters are also shown, and the results from local parameters are retained for nuclei in the dataset. It can be observed that, in the framework of the BFM, parameters from FNN effectively describe the NLD for nuclei both within and beyond the dataset. However, due to the limitations of the Fermi gas model, the parameters from the FNN were unable to capture the details of the NLD variations with excitation energy observed in the Oslo data. For example, in Fig. 10, the experimental NLD data for ^{51}V exhibit oscillations with increasing excitation energy, a pattern that is challenging for the BFM to describe.

IV. SUMMARY AND PROSPECTS

The FNN has been employed to predict parameters of the back-shifted Fermi gas model, including the level density parameter at neutron separation energy $a(S_n)$ and the energy shift Δ . Considering the convenience of data extrapolation, the input for the FNN includes only the proton number Z ,

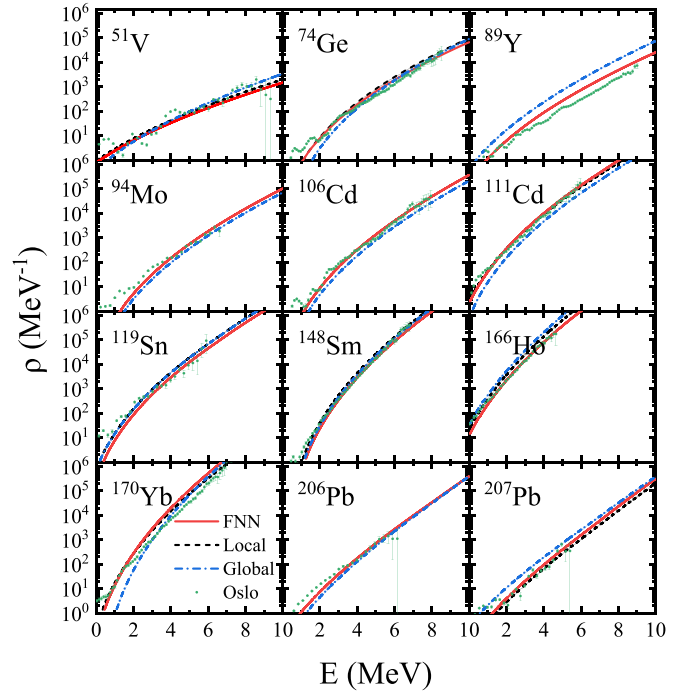


FIG. 10. Comparison among the total NLDs calculated using FNN parameters (red line), local parameters (black dashed line), and global parameters (blue dotted-dashed line) in the BFM with experimental data (green dots with error bars).

neutron number N , and the corresponding difference to the nearest magic number (shell information). For $a(S_n)$, the input is further augmented with the neutron separation energy S_n . The results demonstrate that the FNN effectively reproduces the variation trends of $a(S_n)$. For the energy shift Δ , due to significant differences observed among even-even nuclei, odd-odd nuclei, and odd- A nuclei, three separate neural networks are employed to individually train on each category. The results reveal that the FNN effectively captures the patterns of Δ variation from intermediate to heavy nuclei. However, for lighter nuclei, the data on the original dataset are quite limited, concurrently exhibiting irregular variations, which results in FNN providing less precise descriptions of Δ . This is particularly evident for odd- A nuclei, where the Δ values for nuclei with mass numbers below 80 appear to lack a discernible pattern. This suggests that, at least for lighter nuclei, the FNN may benefit from incorporating additional physical information in the input variables to apply soft constraints on its predictions for Δ . Thanks to the simplicity of the FNN input, extrapolating data becomes straightforward. The FNN provides $a(S_n)$ and Δ values for nearly 3000 nuclei (the detailed parameters can be found in the Supplemental Material [77]). Certainly, for nuclei that are significantly distant from the dataset, caution must be taken when using these parameters.

The calculations of D_0 and D_1 using the parameters obtained from FNN indicate that this set of parameters can effectively describe the experimental data. For D_0 and D_1 , FNN obtains values of f_{rms} as 1.87 and 1.76, respectively. The results suggest that the parameters from FNN achieve a performance close to that of local parameters. The

parameters from FNN also provide a satisfactory description for the 12 nuclei beyond the dataset in RIPL-3, yielding a result of $f_{\text{rms}} = 1.98$. This suggests that the method of providing extrapolated parameters is, at the very least, stable for nuclei close to the dataset. For extrapolated nuclei, in a broader comparison, FNN's D_0 calculation results exhibit patterns similar to those obtained with global parameters. However, there are noticeable differences in certain regions, such as lighter proton-rich nuclei and in the vicinity of ^{100}Sn and ^{132}Sn , where FNN consistently yields smaller results. The calculated results for the cumulative number of levels and NLDs also provide a reasonable description of the experimental data, further affirming the reliability of these parameters.

Overall, in this study, FNN has been employed to discover four sets of function relationships with indeterminate specific forms, enabling a proficient description of existing experimental data through the utilization of exceedingly

simple physical information. In the future, improvements could be achieved by incorporating additional physical information as inputs to the neural network or by considering the utilization of experimental data to impose constraints on the network, aiming for a more accurate description of the parameters. Furthermore, it is also interesting to investigate the impact of level density on the neutron capture process based on the parameters provided by FNN.

ACKNOWLEDGMENTS

This work was supported by the Natural Science Foundation of Jilin Province (Grant No. 20220101017JC), National Natural Science Foundation of China (Grant No. 11675063), Key Laboratory of Nuclear Data Foundation (Grant No. JCKY2020201C157), and Graduate Innovation Fund of Jilin University.

-
- [1] W. Hauser and H. Feshbach, The inelastic scattering of neutrons, *Phys. Rev.* **87**, 366 (1952).
- [2] S. Goriely, S. Hilaire, and A. J. Koning, Improved predictions of nuclear reaction rates with the TALYS reaction code for astrophysical applications, *Astron. Astrophys.* **487**, 767 (2008).
- [3] M. Rajasekaran and V. Devanathan, Nuclear level density and the mass distribution of fission fragments, *Phys. Rev. C* **24**, 2606 (1981).
- [4] C. Yalçın, The cross section calculation of $^{112}\text{Sn}(\alpha, \gamma)^{116}\text{Te}$ reaction with different nuclear models at the astrophysical energy range, *Nucl. Sci. Tech.* **28**, 1 (2017).
- [5] A. Schiller, L. Bergholt, M. Guttormsen, E. Melby, J. Rekdal, and S. Siem, Extraction of level density and γ strength function from primary γ spectra, *Nucl. Instrum. Methods Phys. Res., Sect. A* **447**, 498 (2000).
- [6] A. Spyrou, S. N. Liddick, A.-C. Larsen, M. Guttormsen, K. Cooper, A. C. Dombos, D. J. Morrissey, F. Naqvi, G. Perdikakis, S. J. Quinn *et al.*, Novel technique for constraining r -process (n, γ) reaction rates, *Phys. Rev. Lett.* **113**, 232502 (2014).
- [7] V. W. Ingeberg, S. Siem, M. Wiedeking, K. Sieja, D. Bleuel, C. Brits, T. Bucher, T. Dinoko, J. Easton, A. Gørgen *et al.*, First application of the Oslo method in inverse kinematics, *Eur. Phys. J. A* **56**, 68 (2020).
- [8] M. Wiedeking, M. Guttormsen, A.-C. Larsen, F. Zeiser, A. Gørgen, S. N. Liddick, D. Mũcher, S. Siem, and A. Spyrou, Independent normalization for γ -ray strength functions: The shape method, *Phys. Rev. C* **104**, 014311 (2021).
- [9] H. A. Bethe, An attempt to calculate the number of energy levels of a heavy nucleus, *Phys. Rev.* **50**, 332 (1936).
- [10] H. A. Bethe, Nuclear dynamics, theoretical, *Rev. Mod. Phys.* **9**, 69 (1937).
- [11] A. Gilbert and A. Cameron, A composite nuclear-level density formula with shell corrections, *Can. J. Phys.* **43**, 1446 (1965).
- [12] W. Dilg, W. Schantl, H. Vonach, and M. Uhl, Level density parameters for the back-shifted Fermi gas model in the mass range $40 < A < 250$, *Nucl. Phys. A* **217**, 269 (1973).
- [13] A. V. Ignatyuk, G. N. Smirenkin, and A. S. Tishin, Phenomenological description of energy dependence of the level density parameter, *Yad. Fiz.* **21**, 485 (1975).
- [14] S. Hilaire, J. Delaroche, and M. Girod, Combinatorial nuclear level densities based on the Gogny nucleon-nucleon effective interaction, *Eur. Phys. J. A* **12**, 169 (2001).
- [15] S. Hilaire and S. Goriely, Global microscopic nuclear level densities within the HFB plus combinatorial method for practical applications, *Nucl. Phys. A* **779**, 63 (2006).
- [16] S. Goriely, S. Hilaire, and A. J. Koning, Improved microscopic nuclear level densities within the Hartree-Fock-Bogoliubov plus combinatorial method, *Phys. Rev. C* **78**, 064307 (2008).
- [17] S. Hilaire, M. Girod, S. Goriely, and A. J. Koning, Temperature-dependent combinatorial level densities with the DIM Gogny force, *Phys. Rev. C* **86**, 064317 (2012).
- [18] H. Uhrenholt, S. Åberg, A. Dobrowolski, T. Døssing, T. Ichikawa, and P. Möller, Combinatorial nuclear level-density model, *Nucl. Phys. A* **913**, 127 (2013).
- [19] K.-P. Geng, P.-X. Du, J. Li, and D.-L. Fang, Calculation of microscopic nuclear level densities based on covariant density functional theory, *Nucl. Sci. Tech.* **34**, 141 (2023).
- [20] X. F. Jiang, X. H. Wu, P. W. Zhao, and J. Meng, Nuclear level density from relativistic density functional theory and combinatorial method, *Phys. Lett. B* **849**, 138448 (2024).
- [21] F. N. Choudhury and S. Das Gupta, Nuclear level density with realistic interactions, *Phys. Rev. C* **16**, 757 (1977).
- [22] S. Goriely, A new nuclear level density formula including shell and pairing correction in the light of a microscopic model calculation, *Nucl. Phys. A* **605**, 28 (1996).
- [23] B. Agrawal and A. Ansari, Excitation energy and angular momentum dependence of nuclear level densities and spin cut-off factor in SP and SPA+SPA approaches, *Nucl. Phys. A* **640**, 362 (199A8).
- [24] P. Demetriou and S. Goriely, Microscopic nuclear level densities for practical applications, *Nucl. Phys. A* **695**, 95 (2001).
- [25] J. Zhao, T. Nikšić, D. Vretenar *et al.*, Microscopic model for the collective enhancement of nuclear level densities, *Phys. Rev. C* **102**, 054606 (2020).
- [26] W. Zhang, W. Gao, G.-T. Zhang, and Z.-Y. Li, Level density of odd- A nuclei at saddle point, *Nucl. Sci. Tech.* **34**, 124 (2023).
- [27] V. Zelevinsky, B. A. Brown, N. Frazier, and M. Horoi, The nuclear shell model as a testing ground for many-body quantum chaos, *Phys. Rep.* **276**, 85 (1996).

- [28] J. Wang, S. Dutta, L.-J. Wang, and Y. Sun, Projected shell model description of nuclear level density: Collective, pair-breaking, and multiquasiparticle regimes in even-even nuclei, *Phys. Rev. C* **108**, 034309 (2023).
- [29] W. E. Ormand, Estimating the nuclear level density with the Monte Carlo shell model, *Phys. Rev. C* **56**, R1678 (1997).
- [30] Y. Alhassid, S. Liu, and H. Nakada, Particle-number re-projection in the shell model Monte Carlo method: Application to nuclear level densities, *Phys. Rev. Lett.* **83**, 4265 (1999).
- [31] J. A. White, S. E. Koonin, and D. J. Dean, Shell model Monte Carlo investigation of rare earth nuclei, *Phys. Rev. C* **61**, 034303 (2000).
- [32] Y. Alhassid, G. F. Bertsch, and L. Fang, Nuclear level statistics: Extending shell model theory to higher temperatures, *Phys. Rev. C* **68**, 044322 (2003).
- [33] N. Shimizu, Y. Utsuno, Y. Futamura, T. Sakurai, T. Mizusaki, and T. Otsuka, Stochastic estimation of nuclear level density in the nuclear shell model: An application to parity-dependent level density in ^{58}Ni , *Phys. Lett. B* **753**, 13 (2016).
- [34] J. Chen, M. Liu, C. Yuan, S. Chen, N. Shimizu, X. Sun, R. Xu, Y. Tian *et al.*, Shell-model-based investigation on level density of Xe and Ba isotopes, *Phys. Rev. C* **107**, 054306 (2023).
- [35] R. A. Sen'kov, M. Horoi, and V. G. Zelevinsky, A high-performance fortran code to calculate spin- and parity-dependent nuclear level densities, *Comput. Phys. Commun.* **184**, 215 (2013).
- [36] V. Zelevinsky and M. Horoi, Nuclear level density, thermalization, chaos, and collectivity, *Prog. Part. Nucl. Phys.* **105**, 180 (2019).
- [37] W. E. Ormand and B. A. Brown, Microscopic calculations of nuclear level densities with the Lanczos method, *Phys. Rev. C* **102**, 014315 (2020).
- [38] S. Hilaire, S. Goriely, S. Péru, and G. Gosselin, A new approach to nuclear level densities: The QRPA plus boson expansion, *Phys. Lett. B* **843**, 137989 (2023).
- [39] A. J. Koning, S. Hilaire, and S. Goriely, Global and local level density models, *Nucl. Phys. A* **810**, 13 (2008).
- [40] R. Capote, M. Herman, P. Obložinský, P. Young, S. Goriely, T. Belgya, A. Ignatyuk, A. Koning, S. Hilaire, V. Plujko, M. Avrigeanu, O. Bersillon, M. Chadwick, T. Fukahori, Z. Ge, Y. Han, S. Kailas, J. Kopecky, V. Maslov, G. Reffo *et al.*, RIPL – reference input parameter library for calculation of nuclear reactions and nuclear data evaluations, *Nucl. Data Sheets* **110**, 3107 (2009), Special Issue on Nuclear Reaction Data.
- [41] M. Grossjean and H. Feldmeier, Level density of a Fermi gas with pairing interactions, *Nucl. Phys. A* **444**, 113 (1985).
- [42] V. Plyaskin and R. Kosilov, Level-density parameters in the back-shifted Fermi gas model, *Phys. At. Nucl.* **63**, 752 (2000).
- [43] T. von Egidy and D. Bucurescu, Systematics of nuclear level density parameters, *Phys. Rev. C* **72**, 044311 (2005).
- [44] T. Britton, D. Lawrence, and G. Gavalian, MI track fitting in nuclear physics, *EPJ Web Conf.* **245**, 06015 (2020).
- [45] A. Boehnlein, M. Diefenthaler, N. Sato, M. Schram, V. Ziegler, C. Fanelli, M. Hjorth-Jensen, T. Horn, M. P. Kuchera, D. Lee *et al.*, Colloquium: Machine learning in nuclear physics, *Rev. Mod. Phys.* **94**, 031003 (2022).
- [46] W. He, Q. Li, Y. Ma, Z. Niu, J. Pei, and Y. Zhang, Machine learning in nuclear physics at low and intermediate energies, *Sci. China Phys. Mech. Astron.* **66**, 282001 (2023).
- [47] S. Athanassopoulos, E. Mavrommatis, K. Gernoth, and J. Clark, Nuclear mass systematics using neural networks, *Nucl. Phys. A* **743**, 222 (2004).
- [48] Z. Niu and H. Liang, Nuclear mass predictions based on Bayesian neural network approach with pairing and shell effects, *Phys. Lett. B* **778**, 48 (2018).
- [49] Z. M. Niu, J. Y. Fang, and Y. F. Niu, Comparative study of radial basis function and Bayesian neural network approaches in nuclear mass predictions, *Phys. Rev. C* **100**, 054311 (2019).
- [50] Z.-P. Gao, Y.-J. Wang, H.-L. Lü, Q.-F. Li, C.-W. Shen, and L. Liu, Machine learning the nuclear mass, *Nucl. Sci. Tech.* **32**, 109 (2021).
- [51] X.-C. Ming, H.-F. Zhang, R.-R. Xu, X.-D. Sun, Y. Tian, and Z.-G. Ge, Nuclear mass based on the multi-task learning neural network method, *Nucl. Sci. Tech.* **33**, 48 (2022).
- [52] Z. M. Niu and H. Z. Liang, Nuclear mass predictions with machine learning reaching the accuracy required by r -process studies, *Phys. Rev. C* **106**, L021303 (2022).
- [53] R. Utama, W.-C. Chen, and J. Piekarewicz, Nuclear charge radii: density functional theory meets Bayesian neural networks, *J. Phys. G: Nucl. Part. Phys.* **43**, 114002 (2016).
- [54] Y. Ma, C. Su, J. Liu, Z. Ren, C. Xu, and Y. Gao, Predictions of nuclear charge radii and physical interpretations based on the naive Bayesian probability classifier, *Phys. Rev. C* **101**, 014304 (2020).
- [55] D. Wu, C. L. Bai, H. Sagawa, and H. Q. Zhang, Calculation of nuclear charge radii with a trained feed-forward neural network, *Phys. Rev. C* **102**, 054323 (2020).
- [56] T.-S. Shang, J. Li, and Z.-M. Niu, Prediction of nuclear charge density distribution with feedback neural network, *Nucl. Sci. Tech.* **33**, 153 (2022).
- [57] N. J. Costiris, E. Mavrommatis, K. A. Gernoth, and J. W. Clark, Decoding β -decay systematics: A global statistical model for β^- half-lives, *Phys. Rev. C* **80**, 044332 (2009).
- [58] Z. M. Niu, H. Z. Liang, B. H. Sun, W. H. Long, and Y. F. Niu, Predictions of nuclear β -decay half-lives with machine learning and their impact on r -process nucleosynthesis, *Phys. Rev. C* **99**, 064307 (2019).
- [59] J. Bai, Z. Niu, B. Sun, and Y. Niu, The description of giant dipole resonance key parameters with multitask neural networks, *Phys. Lett. B* **815**, 136147 (2021).
- [60] X. Wang, L. Zhu, and J. Su, Providing physics guidance in Bayesian neural networks from the input layer: The case of giant dipole resonance predictions, *Phys. Rev. C* **104**, 034317 (2021).
- [61] Z. Yuan, D. Tian, J. Li, and Z. Niu, Magnetic moment predictions of odd-A nuclei with the Bayesian neural network approach, *Chin. Phys. C* **45**, 124107 (2021).
- [62] H.-F. Wen, T.-S. Shang, J. Li, Z.-M. Niu, D. Yang, Y.-H. Xue, X. L. Li, and X.-L. Huang, Prediction of ground-state spin in odd-A nuclei within decision tree, *Acta Phys. Sin.* **72**, 152101 (2023).
- [63] Y. Wang, X. Zhang, Z. Niu, and Z. Li, Study of nuclear low-lying excitation spectra with the Bayesian neural network approach, *Phys. Lett. B* **830**, 137154 (2022).
- [64] S. Akkoyun, H. Kaya, and Y. Torun, Estimations of first 2^+ energy states of even-even nuclei by using artificial neural networks, *Indian J. Phys.* **96**, 1791 (2022).
- [65] C.-W. Ma, D. Peng, H.-L. Wei, Z.-M. Niu, Y.-T. Wang, and R. Wada, Isotopic cross-sections in proton induced spallation

- reactions based on the Bayesian neural network method, *Chin. Phys. C* **44**, 014104 (2020).
- [66] D. Peng, H.-L. Wei, X.-X. Chen, X.-B. Wei, Y.-T. Wang, J. Pu, K.-X. Cheng, and C.-W. Ma, Bayesian evaluation of residual production cross sections in proton-induced nuclear spallation reactions, *J. Phys. G: Nucl. Part. Phys.* **49**, 085102 (2022).
- [67] J. Keeble and A. Rios, Machine learning the deuteron, *Phys. Lett. B* **809**, 135743 (2020).
- [68] C. Adams, G. Carleo, A. Lovato, and N. Rocco, Variational monte carlo calculations of $A \leq 4$ nuclei with an artificial neural-network correlator ansatz, *Phys. Rev. Lett.* **127**, 022502 (2021).
- [69] L.-J. Guo, J.-Y. Xiong, Y. Ma, and Y.-L. Ma, Insights into neutron star equation of state by machine learning, *Astrophys. J.* **965**, 47 (2024).
- [70] H. Özdoğan, Y. A. Üncü, M. Şekerci, and A. Kaplan, Estimations of level density parameters by using artificial neural network for phenomenological level density models, *Appl. Radiat. Isot.* **169**, 109583 (2021).
- [71] Z.-X. Yang, X.-H. Fan, P. Yin, and W. Zuo, Taming nucleon density distributions with deep neural network, *Phys. Lett. B* **823**, 136650 (2021).
- [72] Z.-X. Yang, X.-H. Fan, T. Naito, Z.-M. Niu, Z.-P. Li, H. Liang *et al.*, Calibration of nuclear charge density distribution by back-propagation neural networks, *Phys. Rev. C* **108**, 034315 (2023).
- [73] N. Hizawa, K. Hagino, and K. Yoshida, Analysis of a Skyrme energy density functional with deep learning, *Phys. Rev. C* **108**, 034311 (2023).
- [74] W. Li, X. Zhang, Y. Niu, and Z. Niu, Comparative study of neural network and model averaging methods in nuclear β -decay half-life predictions, *J. Phys. G: Nucl. Part. Phys.* **51**, 015103 (2024).
- [75] H. Robbins and S. Monro, A stochastic approximation method, *Ann. Math. Stat.* **22**, 400 (1951).
- [76] A. Koning and D. Rochman, Modern nuclear data evaluation with the TALYS code system, *Nucl. Data Sheets* **113**, 2841 (2012), Special Issue on Nuclear Reaction Data.
- [77] See Supplemental Material at <http://link.aps.org/supplemental/10.1103/PhysRevC.109.044325> for all parameters provided by the FNN.
- [78] A. C. Larsen, R. Chankova, M. Guttormsen, F. Ingebretsen, S. Messelt, J. Rekstad, S. Siem, N. U. H. Syed, S. W. Ødegård, T. Lönnroth, A. Schiller, and A. Voinov, Microcanonical entropies and radiative strength functions of $^{50,51}\text{V}$, *Phys. Rev. C* **73**, 064301 (2006).
- [79] T. Renstrøm, H.-T. Nyhus, H. Utsunomiya, R. Schwengner, S. Goriely, A. C. Larsen, D. M. Filipescu, I. Gheorghe, L. A. Bernstein, D. L. Bleuel, T. Glodariu, A. Görgen, M. Guttormsen, T. W. Hagen, B. V. Kheswa, Y.-W. Lui, D. Negi, I. E. Ruud, T. Shima, S. Siem *et al.*, Low-energy enhancement in the γ -ray strength functions of $^{73,74}\text{Ge}$, *Phys. Rev. C* **93**, 064302 (2016).
- [80] A. C. Larsen, M. Guttormsen, R. Schwengner, D. L. Bleuel, S. Goriely, S. Harissopulos, F. L. Bello Garrote, Y. Byun, T. K. Eriksen, F. Giacoppo, A. Görgen, T. W. Hagen, M. Klintefjord, T. Renstrøm, S. J. Rose, E. Sahin, S. Siem, T. G. Tornyi, G. M. Tveten, A. V. Voinov *et al.*, Experimentally constrained $(p, \gamma)^{89}\text{Y}$ and $(n, \gamma)^{89}\text{Y}$ reaction rates relevant to p -process nucleosynthesis, *Phys. Rev. C* **93**, 045810 (2016).
- [81] H. Utsunomiya, S. Goriely, T. Kondo, C. Iwamoto, H. Akimune, T. Yamagata, H. Toyokawa, H. Harada, F. Kitatani, Y.-W. Lui *et al.*, Photoneutron cross sections for Mo isotopes: A step toward a unified understanding of (γ, n) and (n, γ) reactions, *Phys. Rev. C* **88**, 015805 (2013).
- [82] A.-C. Larsen, I. E. Ruud, A. Bürger, S. Goriely, M. Guttormsen, A. Görgen, T. W. Hagen, S. Harissopulos, H. T. Nyhus, T. Renstrøm *et al.*, Transitional γ strength in Cd isotopes, *Phys. Rev. C* **87**, 014319 (2013).
- [83] H. K. Toft, A. C. Larsen, U. Agvaanluvsan, A. Bürger, M. Guttormsen, G. E. Mitchell, H. T. Nyhus, A. Schiller, S. Siem, N. U. H. Syed *et al.*, Level densities and γ -ray strength functions in Sn isotopes, *Phys. Rev. C* **81**, 064311 (2010).
- [84] S. Siem, M. Guttormsen, K. Ingeberg, E. Melby, J. Rekstad, A. Schiller, and A. Voinov, Level densities and γ -strength functions in $^{148,149}\text{Sm}$, *Phys. Rev. C* **65**, 044318 (2002).
- [85] F. Pogliano, F. L. Bello Garrote, A. C. Larsen, H. C. Berg, D. Gjestvang, A. Görgen, M. Guttormsen, V. W. Ingeberg, T. W. Johansen, K. L. Malatji, E. F. Matthews, M. Markova, J. E. Midtbø, V. Modamio, L. G. Pedersen, E. Sahin, S. Siem, T. G. Tornyi, and A. S. Voyles, Observation of a candidate for the $M1$ scissors resonance in odd-odd ^{166}Ho , *Phys. Rev. C* **107**, 034605 (2023).
- [86] U. Agvaanluvsan, A. Schiller, J. A. Becker, L. A. Bernstein, P. E. Garrett, M. Guttormsen, G. E. Mitchell, J. Rekstad, S. Siem, A. Voinov, and W. Younes, Level densities and γ -ray strength functions in $^{170,171,172}\text{Yb}$, *Phys. Rev. C* **70**, 054611 (2004).
- [87] N. U. H. Syed, M. Guttormsen, F. Ingebretsen, A. C. Larsen, T. Lönnroth, J. Rekstad, A. Schiller, S. Siem, and A. Voinov, Level density and γ -decay properties of closed shell Pb nuclei, *Phys. Rev. C* **79**, 024316 (2009).